Available online at www.sciencedirect.com
SCIENCE DIRECT
ELSEVIER
European Journal of Mechanics B/Fluids 25 (2006) 379–392
EUROPEAN JOURNAL OF MECHANICS B/FLUIDS

Numerical simulation of unsteady blade row interactions induced by passing wakes

Pascale Kulisa *, Cédric Dano

LMFA UMR 5509, Ecole Centrale de Lyon, 36, av. Guy de Collongue, BP 163, 69134 Ecully cedex, France

Received 29 November 2004; received in revised form 7 April 2005; accepted 6 August 2005

Available online 19 December 2005

Abstract

A numerical study of the unsteady phenomena resulting of periodic passing wakes is presented. An unsteady passing wake boundary condition is implemented in a three-dimensional Navier–Stokes code. Unsteady computations are performed to evaluate the capability of the code to simulate the rotor–stator interaction flow. The analysis of the flow structures shows the vortical disturbances and the migration of the incoming wakes through the blade passage. This physical analysis allows to separate the main origins of the losses.

Keywords: Rotor–stator interaction; Numerical simulation; Wake

1. Introduction

In turbomachinery, the physical phenomena are numerous and complex. The fluid is strongly deviated and undergoes significant pressure and temperature variations. Many swirling structures appear and interact together. Performance improvement requires to load the blade by decreasing the blade number and to reduce the row spacing [1–3]. Interactions between adjacent blade rows are consequently increased. The aerodynamic blade load increase emphasises the separated zones appearance. Unsteady phenomena resulting from the periodic wakes due to the upstream blade row appear to be crucial, [4]. The turbulence modelling is also important to provide accurate numerical simulations. This fact is emphasised when heat transfer exists as it is the case for the turbine flows [5]. A RANS (Reynolds Averaged Navier–Stokes) approach is mainly used in turbomachinery because the geometry configurations are complex and the Reynolds number is high.

The present study evaluates the ability to reproduce the rotor–stator interactions phenomena without simulating the complete stage configuration and analyses the main origin of the losses in a turbine configuration. The computation is limited to a single stator passage. A boundary condition of passing wakes is prescribed to reproduce the unsteady effects of incoming wakes. The first part of the study consists in evaluating different two-equation turbulence models for turbomachinery applications. The objective is to select one model which is efficient for the blade wake prediction and sufficiently robust for the application area. Numerous steady computations were performed for turbine and

* Corresponding author. Fax: +33 (0)4 78 64 71 45.
E-mail address: pascale.kulisa@ec-lyon.fr (P. Kulisa).

0997-7546/$ – see front matter
doi:10.1016/j.euromechflu.2005.08.001

compressor test cases. The *k–l* model of Smith was retained. This first part was presented in details in [6]. The second part consists in simulating the rotor–stator interaction phenomena using an unsteady boundary condition. The present paper concerns this second part. The method is explained and we focus on flow structures occurring within the wake-blade interaction.

When the wakes of an upstream blade row progress through the downstream blade passage, characteristic pattern of vortical structure is created. The incoming wakes are cut and convected through the passage. A vortical flow is then produced at each side of the leading edge. Moreover, the wakes migrate towards the suction surface for a turbine (towards the pressure side for a compressor). The two vortical structures evolve differently on the suction side or on the pressure side of the blade.

On the pressure side, the incoming wake evolves into counter-rotating vortices. These vortices are the dominant source of disturbances over the blade pressure side. On the suction side, the flow is characterised by a vortical stream induced by the wake impact on the leading edge. The boundary layer on the suction side is distorted and aspirated from the surface.

Computations are performed with the Canari numerical code developed by Onera. This code solves the averaged three-dimensional Navier–Stokes compressible equations. The turbulence model used for this simulation is the low-Reynolds number two-equation model *k–l* developed by Smith [7]. A non-linear approach, avoiding the Boussinesq hypothesis, is used.

The steady computational procedure has been validated by experimental data comparisons on various turbine and compressor configurations [6]. In the present study, the wake propagation is evaluated in a high subsonic turbine cascade. The experimental conditions are close to those encountered in the real engine. Because the velocity level is high and the blade boundary layers are thin, detailed aerodynamic data in the blade passage are not available. The interest of this test case is to evaluate the ability of the method in complex and realistic turbine configuration. The stagnation pressure distribution downstream the blade is compared to measurements. Then the unsteady flow structures generated by the incoming moving wakes are analysed. For turbine cases, the interpretation of these unsteady effects has been discussed in [8–10]. We show that the physical phenomena taking place in the rotor–stator interaction are reproduced by this method. So this approach may be an efficient compromise between steady calculations and unsteady stage calculations.

2. Experimental configuration

The experimental configuration concerns the flow developing in a linear turbine cascade. The experimental study was carried out in the von Karman Institute piston compression tube facility [11], Fig. 3. The complete description of the wind tunnel is presented in [12]. This facility is made of three main parts: a 5 meter long and 1 meter diameter cylinder, the test section, and a downstream dump tank. The cylinder contains a lightweight piston driven by the air coming from a high pressure reservoir. As the piston is pushed forward, the gas located in front of it is isentropically compressed until it reaches the requested pressure and temperature levels. The valve is then opened, allowing the pressurised and heated gas to flow through the test section. The freestream conditions (total temperature, pressure, mass flow) are constant. The exit Mach number (about 0.8), Reynolds number and the freestream to wall temperature ratio can be adjusted independently. A steady flow condition is maintained during 500 ms. The total pressure is obtained by 3-hole probe mounted on a pneumatic traversing system located downstream of the blade. The measurements are performed at midspan. The pressure measurements present an uncertainty of ± 1 mbar. The heat flux uncertainty is $\pm 5\%$. To generate the incoming wakes, a rotating disc is set in front of the blade cascade. Cylinders are fixed on the disc diameter.

The main interest of this experiment is to provide realistic conditions near to the real engine. The price to pay is that only global quantities may be measured. So the present study allows to validate the approach in a complex situation.

3. Physical model and turbulence modelling

The physical model of the flow is based on the compressible three-dimensional Navier–Stokes equations. The governing system is composed by the conservation equations of the density, the momentum and the energy. These Reynolds averaged equations involves unknown correlations: the Reynolds stresses and the turbulent heat transfer. To close the energy equation, the turbulent thermal diffusivity is related to the eddy viscosity by a constant turbulent

Prandtl number. In order to close the averaged Navier–Stokes equations, the Reynolds stresses have to be related to the mean velocity gradients. This relation leads to determine two turbulent scales. The first scale is the turbulent kinetic energy k (or q^2 defined by $q^2 = 2k$) and the second one is often ε, the dissipation rate of k. Smith [13] proposes a linear model which is directly based on a length scale l, defined by $k^{3/2}/\varepsilon$. Two supplementary transport equations for k and l are solved. These equations may be written as:

$$\frac{D(\bar{\rho}q^2)}{Dt} = 2Pk - \frac{2\rho q^3}{B_1 l} - 2\mu q_{,i} q_{,j} + \left[(\mu + S_q \mu_t) q^2_{,i}\right]_{,i}, \tag{1}$$

$$\frac{D\rho l}{Dt} = (2 - E_2)\frac{\rho q}{B_1}\left[1 - \left(\frac{l}{\kappa y}\right)^2\right] - \frac{\mu_t}{l} S_q l_{,i} l_{,i} \left(\frac{l}{\kappa y}\right)^2 + 2S_q \left(\frac{\mu_t}{q^2}\right) l_{,i} q^2_{,i} + \left[(\mu + S_q \mu_t) l_{,i}\right]_{,i} \tag{2}$$

where y is the distance to the wall. The turbulent viscosity μ_t is expressed by:

$$\mu_t = \mu \chi \phi, \tag{3}$$

$$\chi = \frac{\rho q l}{\mu B_1^{1/3}}, \tag{4}$$

$$\phi = \left(\frac{C_1^4 f_1 + C_2^2 \chi^2 + \chi^4}{C_1^4 + C_2 \chi^2 + \chi^4}\right)^{1/4}, \tag{5}$$

$$f_1 = \exp\left(-50 \frac{l^2}{\kappa y}\right) \tag{6}$$

with $B_1 = 18$, $S_q = 0.7$, $C_1 = 25.5$, $C_2 = 2.0$, $E_1 = 2.0$, $E_2 = 1.2$ and $\kappa = 0.41$.

A non-linear $k - l$ model was developed by Speziale [14]. Using the invariants theory in continuum mechanics, constitutive relations for the Reynolds stresses are expressed, depending only on the mean velocity gradients and the turbulent scales. The non-linear k–l model differs from the linear one by the addition of two terms in the expression of τ_{ij}. These two terms are quadratic for the mean velocity gradients. The non-linear model is implemented in the Navier–Stokes code. Coefficients and near-wall damping functions used in the equations of k (or q^2) and l are unchanged. The new expression of the Reynolds stresses is:

$$\tau_{ij} = -\frac{2}{3}\rho k \delta_{ij} + 2\mu_{t(Smith)} \overline{S^*_{ij}} + \gamma_1 \left(\overline{S}_{im}\overline{S}_{mj} - \frac{1}{3}\overline{S}_{mn}\overline{S}_{mn}\delta_{ij}\right) + \gamma_2 \left(\overset{\circ}{\overline{S}}_{ij} - \frac{1}{3}\overset{\circ}{\overline{S}}_{mm}\delta_{ij}\right) \tag{7}$$

with

$$\overline{S^*_{ij}} = \overline{S}_{ij} - \frac{1}{3}\overline{S}_{kk}\delta_{ij}, \tag{8}$$

$$\overline{S}_{ij} = \frac{1}{2}\left(\frac{\partial \overline{u}_i}{\partial x_j} + \frac{\partial \overline{u}_j}{\partial x_i}\right), \tag{9}$$

$$\overset{\circ}{\overline{S}}_{ij} = \frac{\partial \overline{S}_{ij}}{\partial t} + u_k \cdot \nabla \overline{S}_{ij} - \frac{\partial \overline{u}_i}{\partial x_k}\overline{S}_{kj} - \frac{\partial \overline{u}_j}{\partial x_k}\overline{S}_{ki}, \tag{10}$$

$$\gamma_1 = 4 C_D C_\mu^2 \rho l, \tag{11}$$

$$\gamma_2 = 4 C_E C_\mu^2 \rho l, \tag{12}$$

$$C_D = C_E = 1.68,$$

$$C_\mu = 0.09.$$

4. Numerical approach

The numerical code used for this study is the Canari solver developed by Onera [15] and validated for external aerodynamic and turbomachinery configurations. The code solves the compressible three-dimensional Navier–Stokes equations with a finite volume approach. The unsteady terms are treated by a four-step Runge–Kutta temporal scheme. The spatial terms are discretized by a Roe's scheme and the viscous terms by a 2nd order centred scheme. Second

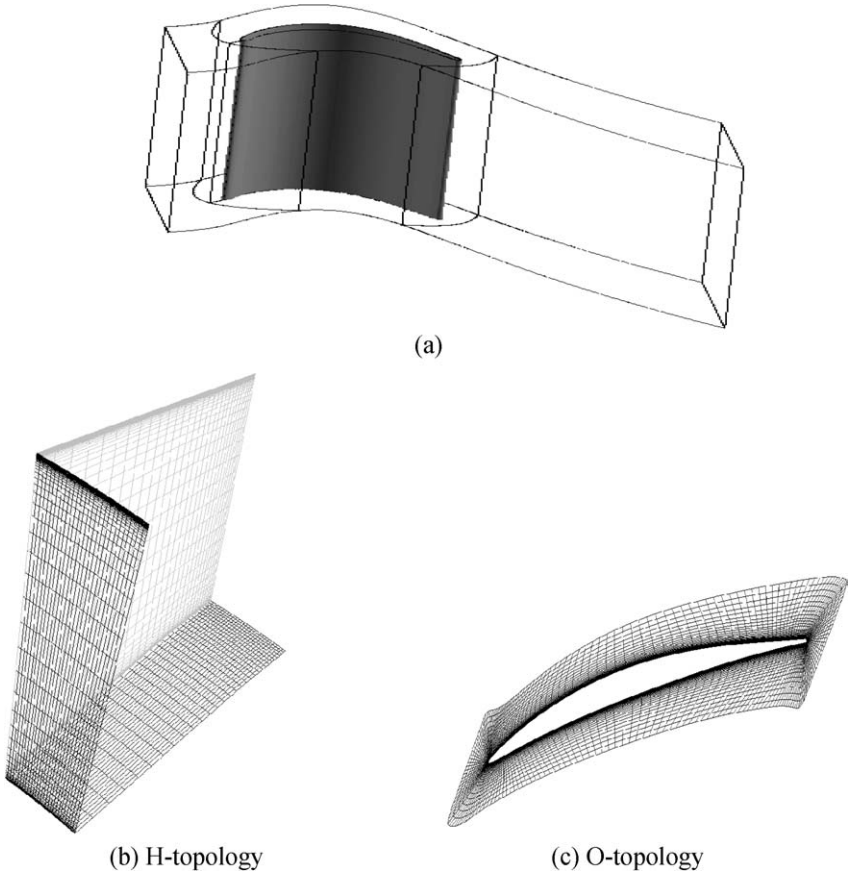

Fig. 1. Mesh.

and fourth dissipative terms are added to ensure numerical stability. An implicit residual smoothing is implemented to accelerate the convergence.

A multi-domain approach on structured meshes is used with classical H–O–H topology, Fig. 1. Two H-grids describe the upstream and the downstream of the cascade, Fig. 1(b). An O-grid is defined around the blade to allow a precise description of the near-wall and the leading edge regions, Fig. 1(c). The mesh contains around 2 10^6 nodes ($H_{upstream}$: 254 975 nodes, O: 1 154 279 nodes, $H_{downstream}$: 594 941 nodes). A previous study [16] on the behaviour of the code for steady thermal test cases showed that the non-dimensional wall distance y^+ must be less than 1 for two-equation models. The first cell size around the blade is $y^+ = 0.2$ in our study. In order to verify the capture of the turbulent gradients, assessment of k-equation is presented Fig. 2 for two streamwise positions on the blade pressure side, at axial mid-chord and just upstream the trailing edge. The global behaviour of the different terms is well reproduced. Outside the boundary layer, the production term balances the dissipation. Near the wall, the production and the turbulent diffusion tend towards zero. The molecular diffusion term plays the major rule and balances the dissipation. We notice that the mesh refinement is sufficient to carry out the gradients of the turbulent terms.

For unsteady applications, the time step is of the order of magnitude of the space cell size. A recent work [17] on the convergence mesh with the Canari code concludes that the results are independent of the mesh when the y^+ is up to 4. So we can conclude that the mesh used for this application is sufficiently fine ($y^+ = 0.2$) to produce accurate results. On the other hand, the mesh may not be too fine because this leads to an important increase of the computational time. The upstream passing wakes are observed during 6 periods which ensure a complete description of the phenomena. The three-dimensional simulation needs 5 CPU hours on a NEC SX5 computer.

According to a subsonic flow, total pressure, total temperature and flow angles are prescribed at the inlet of the domain. The turbulent inlet conditions are determined from a turbulence rate and a characteristic length scale. The

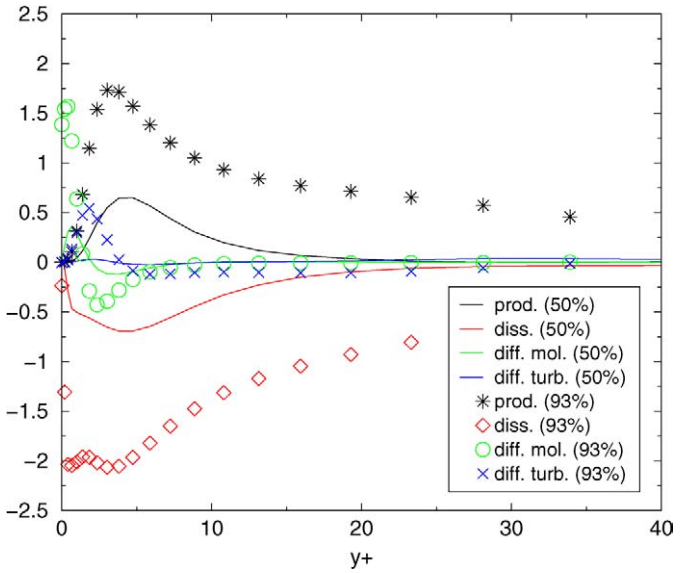

Fig. 2. Assessment of k-equation on the blade pressure side.

turbulent kinetic energy is then deduced using the Bradshaw's relation:

$$k_\infty = \frac{3}{2}(Tu_\infty U_\infty)^2. \tag{13}$$

The freestream turbulence intensity is equal to 10% and the length scale is fixed to 1% of the blade pitch.

The static pressure is given in the outlet section. At the blade wall, non-slip and isothermal conditions are prescribed. The difference between the inlet gas temperature and the wall temperature is about 100 K.

The particularity of the study is the presence of upstream passing bars, taken into account through an unsteady boundary condition. This condition is detailed in the next paragraph.

The convergence is observed through the mass flow conservation. The difference between the upstream and the downstream sections must be less than 1%. Moreover, the mass flow is conserved between two time periods after 6 periods.

5. Passing wakes modelisation

The unsteady effects of incoming wakes are modelled by an inlet boundary condition. This method allows to reduce the computational domain to one blade row. Moreover, if the rotor–stator blade count ratio is set to 1:1, the computational domain may be reduced to a single blade passage.

The incoming wake is described by a similarity law proposed by Lakshminarayana and Davino [18]. This law gives the aerodynamic variables on each node of the upstream surface and describes the spatial evolutions by a Gaussian function. The spatial evolution of the total pressure is given by:

$$P_\mathrm{T} = \overline{P_\mathrm{T}}\left\{1 - \delta p \exp\left[-\alpha\left(\frac{y}{L/2}\right)^2\right]\right\} \tag{14}$$

with the definitions: $\overline{P_\mathrm{T}}$, mean total pressure, δp, pressure defect, $\alpha = 0.693$, $L =$ wake width, y, azimuthal coordinate.

In our test case, the total pressure defect is fixed at 13.6% and the width is 20% of the blade pitch, in accordance of the experimental conditions. The particular attention given to the density of the upstream mesh ensures an accurate transport of the wake and avoids numerical dissipation.

An azimuthal moving is added for temporal evolution. At each time step, the wake is translated in the azimuthal direction with a constant velocity U. For each node and at each time step, the spatial-temporal wake law gives the level of the aerodynamic quantities prescribed in the inlet boundary surface. The incoming wake transport is then

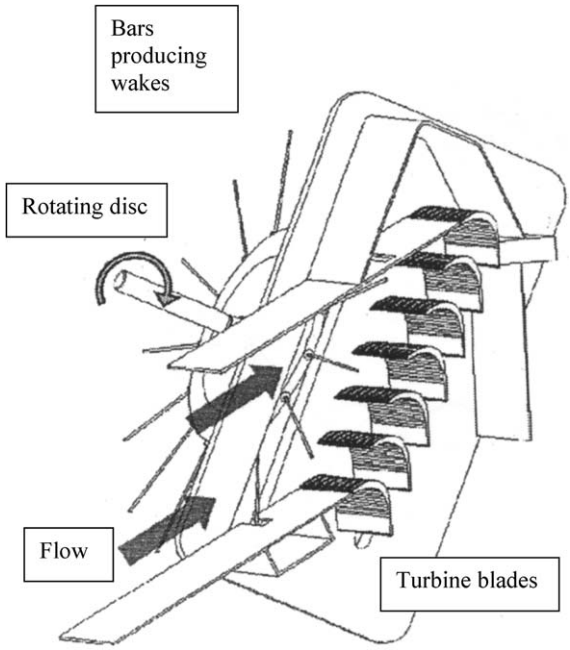

Fig. 3. VKI test facility.

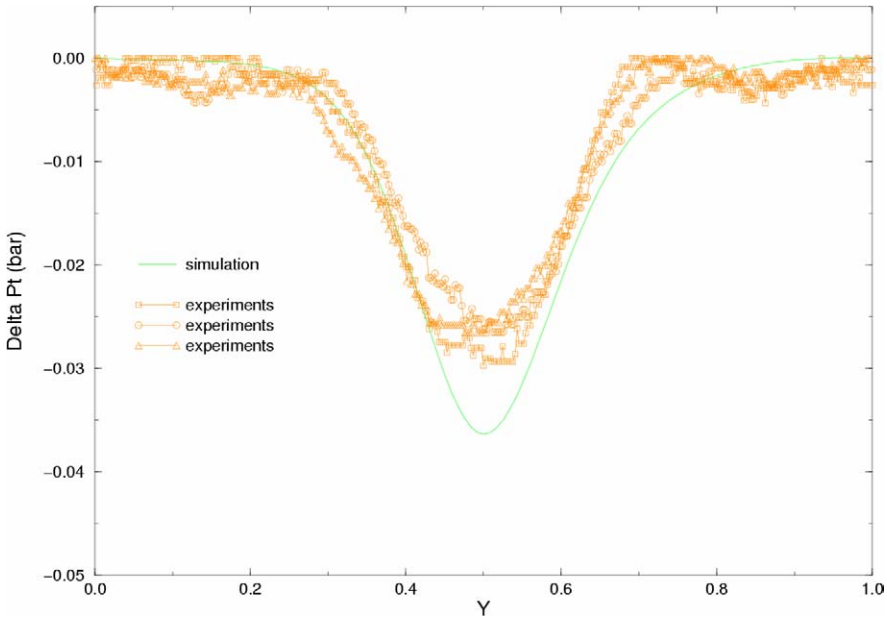

Fig. 4. Wake profile downstream of the blade.

characterised by a velocity defect which is convected in the computational domain. This wake model was implemented in the solver.

6. Flow analysis

Steady computations are first performed and comparisons are made with experimental results. The total pressure defect profile is presented in Fig. 4, downstream of the blade at 140% of the axial chord. Y is the distance in the blade

to blade direction divided by the cascade pitch. The numerical results are in a good agreement with the experimental one. In the central part of the wake, the calculation overestimates the total pressure defect.

The flow structures are analysed in Fig. 5 at mid-span. Among the time steps describing a full time period, eight are extracted and presented to visualise the flow evolution. The wake is a region of losses and the entropy is an appropriate quantity to visualise the wake transport. Hereafter, we call "incoming wake" the upstream wake generated by the cylinders and "blade wake" the wake produced at the blade trailing edge.

The potential effect induced by the blade decelerates the incoming wake in the axial direction. The deviation increases. In the blade passage, the acceleration of the flow leads to the aspiration of the incoming wake. It is cut by the blade and convected to the suction side of the blade. This is due to the tangential velocity defect. This typical phenomenon is illustrated in Fig. 6. We consider two particles: one particle outside of the wake, moving with a velocity level V_1 and an other particle inside of the wake, moving with a lower velocity V_2. Because of the rotation velocity, the second particle presents, in the rotor frame, a tangential velocity excess which leads to a slip-velocity V_g. As a consequence, the upstream wake is seen as a "negative jet" by the second row, [19].

We notice an entropy accumulation on the blade suction side. This reveals that the boundary layers are strongly influenced by the periodic passing of the wakes. After convection to the trailing edge, the two regions interact with the blade wake. The computed results are in good agreement with the experimental observations of Hodson and Dawes [20,21]. These authors showed the bowing and the shearing of the incoming wake through the turbine passage and conclude that these phenomena are mainly governed by convective mechanisms. Our observations fit very well with the numerical results of Cardamone [22] obtained on a similar turbine cascade configuration with a passing cylinder wake.

Stagnation pressure visualisations give more details on the interactions in Fig. 7. The upstream incoming wake is cut and then is divided in two zones of losses which develop independently in the passage. On the suction side, we find the loss accumulation, already observed on the entropy, which interacts with the blade wake. On the pressure side, the incoming wake remains locked in the low velocity region. This part is then convected to the trailing edge and interacts with the blade wake. So, these two parts arrive near the trailing edge at different times. This dissymmetric phenomenon induces a beat of the blade wake. Similar observations are made by Casciaro [23] on a turbine cascade configuration with a same total pressure level.

7. Velocity fluctuations

We have also subtracted the time averaged solution to the unsteady one to deduce the velocity fluctuations. The results are presented in a plane located at mid-span, Fig. 8, for the same 8 time steps. The velocity vectors are associated to the velocity fluctuation direction and the isolines give the fluctuation module. The interaction with the passing wake generates two counter-rotating vortices. These two vortices are stretched in the inter-blade passage and take the full blade to blade space. Between the vortices, the velocity defect produces the particle slip from the pressure side to the suction side. The maximal level of the velocity fluctuations, near the leading edge, reaches 12% of the inlet velocity. The level is in agreement with the observations of Hodson [4]. The vortice, located downstream the incoming wake, generates fluctuation levels on the blade surfaces of the order of magnitude of those encountered in the blade wake. For each passing wake in the passage, we can observe the double interaction with the boundary layers: first with the vortice downstream of the incoming wake and then with the wake itself. At the trailing edge these interaction zones interact with the blade wake.

The losses are defined by

$$\varsigma = 1 - \frac{1 - (P_2/P_{02})^{(\gamma-1)/\gamma}}{1 - (P_2/P_{01})^{(\gamma-1)/\gamma}}$$

where P_2 and P_{02} are the static and the stagnation pressure at the considered point and P_{01} is the stagnation pressure upstream of the blade. The different losses regions are identified. Fig. 9 presents the losses in a cutting plane ($x =$ constant) located just downstream the trailing edge. The three-dimensional nature of the flow is observed. The lateral boundary layers are 15% of the blade spanwise direction and generate the passage vortex. We identify the passage vortex and the loss induced by the incoming wake. We can observe that the losses produced by the incoming wake have a lower level than those produced by the passage vortex.

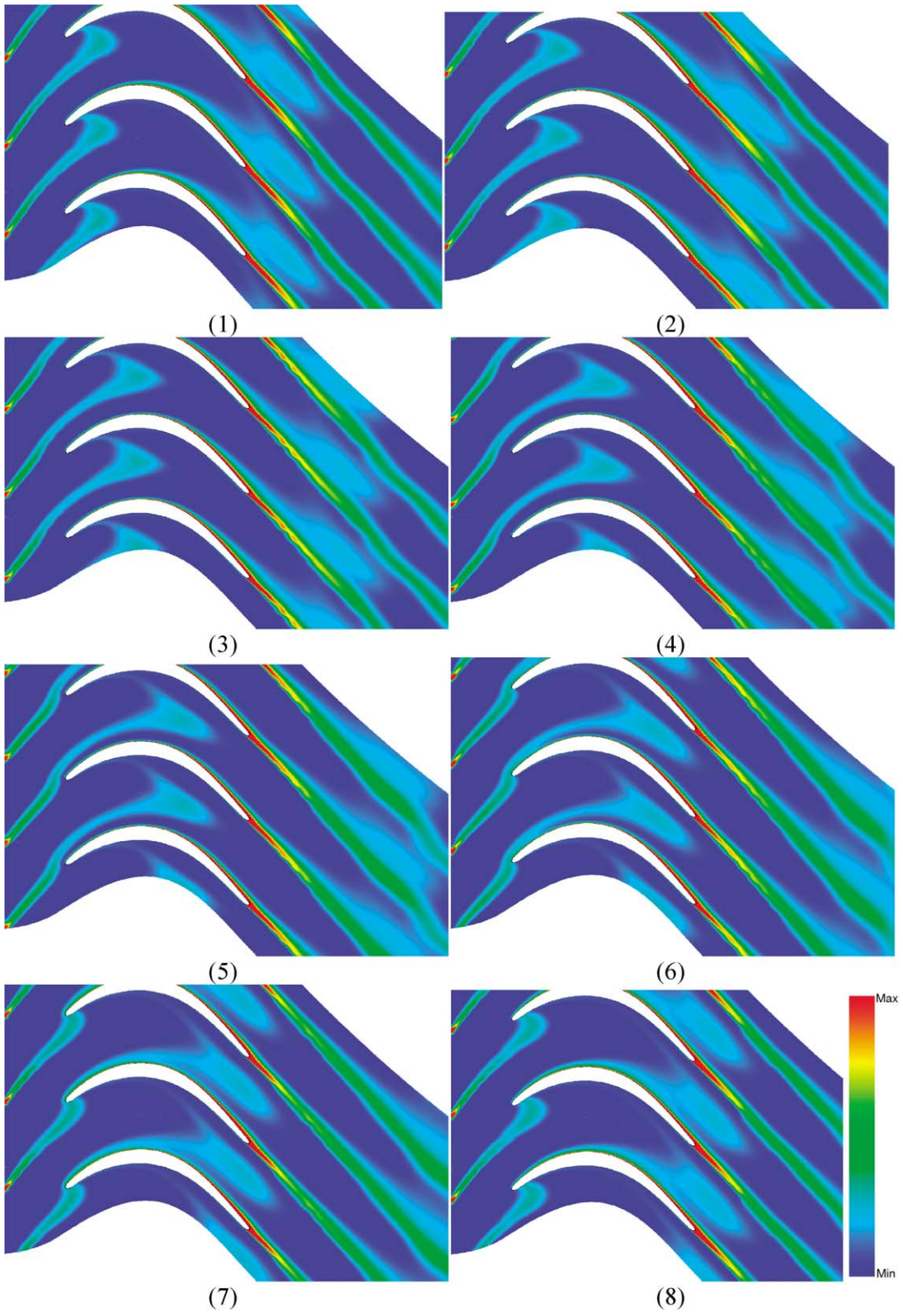

Fig. 5. Entropy evolutions during a full time period.

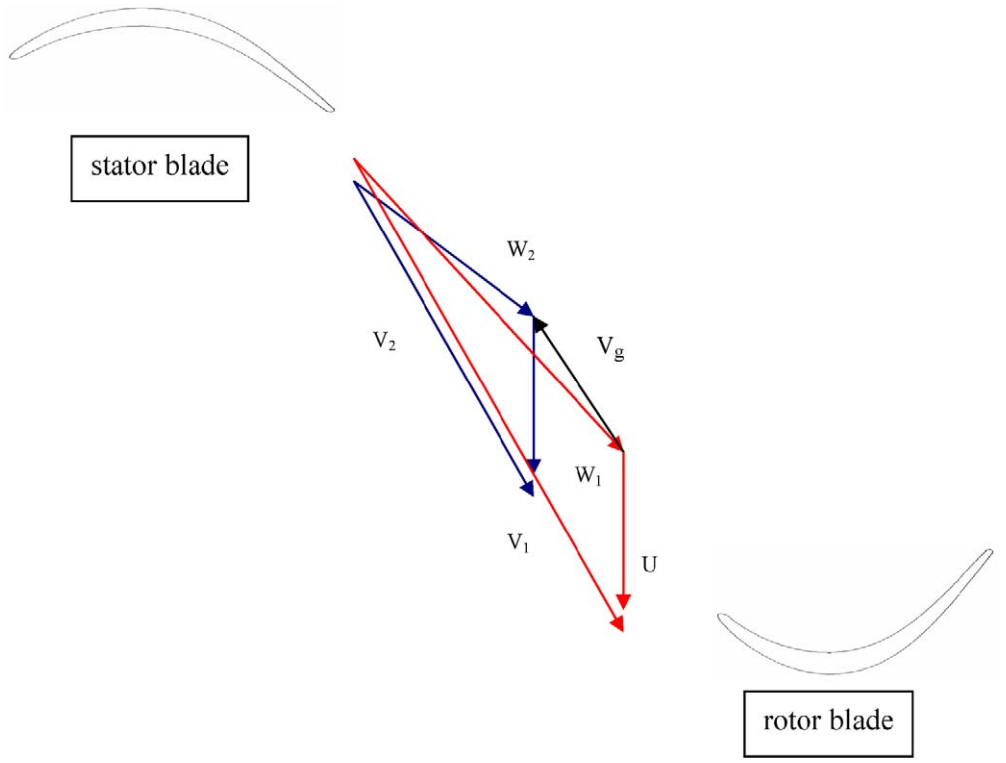

Fig. 6. "Negative jet" structure.

We compare Fig. 10 the losses behind the trailing edge obtained for the steady simulation (without passing wake) and those obtained from the time-averaged results with incoming wakes. The flow presents the same structures in the two cases, but the extend and the intensity of the maximum loss region are increased. We notice that the losses in the blade wake are strongly increased at midspan. Near the endwall, the passage vortex remains the dominant structure which keeps a quasi-steady behaviour, in spite of the incoming wake. The same conclusions are given by Casciaro [23]. From numerical studies, they observed that the passage vortex is lifted by the passing wake but keep stable during the time, showing that this vortex structure is only slightly influenced by the incoming wake. The lift of the passage vortex leads to a modification of the loss production. The same conclusions are obtained by Boletis [8] from experimental data. The influence of the incoming wake on the passage vortex generation is visualised Fig. 11. The three-dimensional entropy is presented in two cutting planes: at 30% of the chord downstream the leading edge and in the wake. The growing and lifting of the passage vortex is observed. The incoming wake remains two-dimensional in the center part of the blade passage. On the contrary, near the endwall, a strong mixing exists but the passage vortex remains the dominant phenomenon leading to the loss generation.

To complete the analysis, we can observe, Fig. 11, an other high loss region just at the endwall. This region corresponds to the corner vortex, generated by the interaction of the blade boundary layer and the endwall boundary layer. This flow region is not affected by the incoming wake.

8. Conclusions

A passing wake boundary condition was implemented in the three-dimensional Navier–Stokes code Canari. Unsteady computations are performed for a realistic turbine case close to the real engine conditions. The ability of the method to simulate the rotor–stator interaction flow is evaluated. The main structures of the flow resulting of the interaction between the passage flow and the incoming wakes are well reproduced and in agreement with the literature results.

The passing wakes are cut by the leading edge and the two parts are convected through the blade passage. The main phenomena are connected to the velocity defect of the passing wake which leads to the flow azimuthal transport from

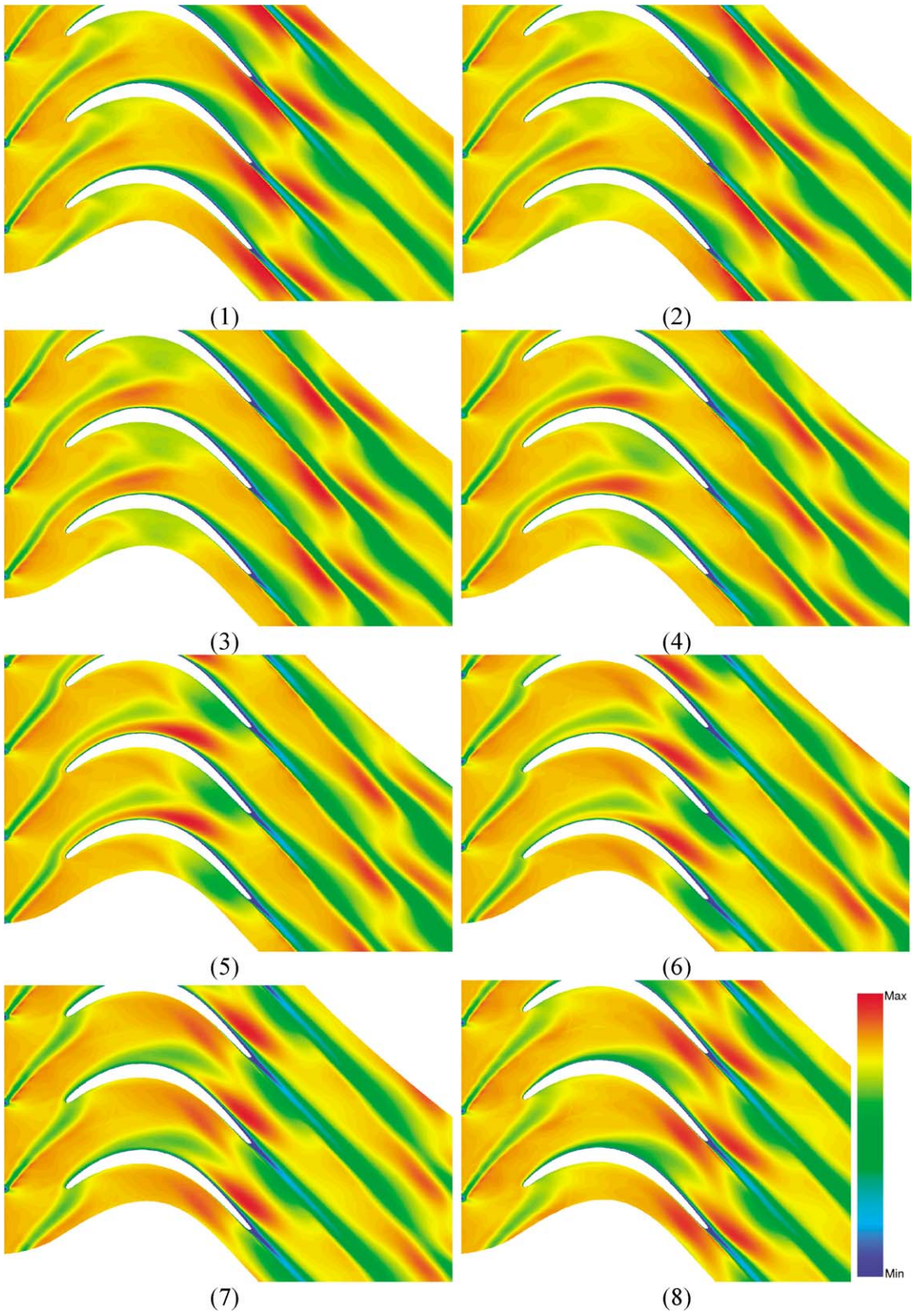

Fig. 7. Stagnation pressure evolutions during a full time period.

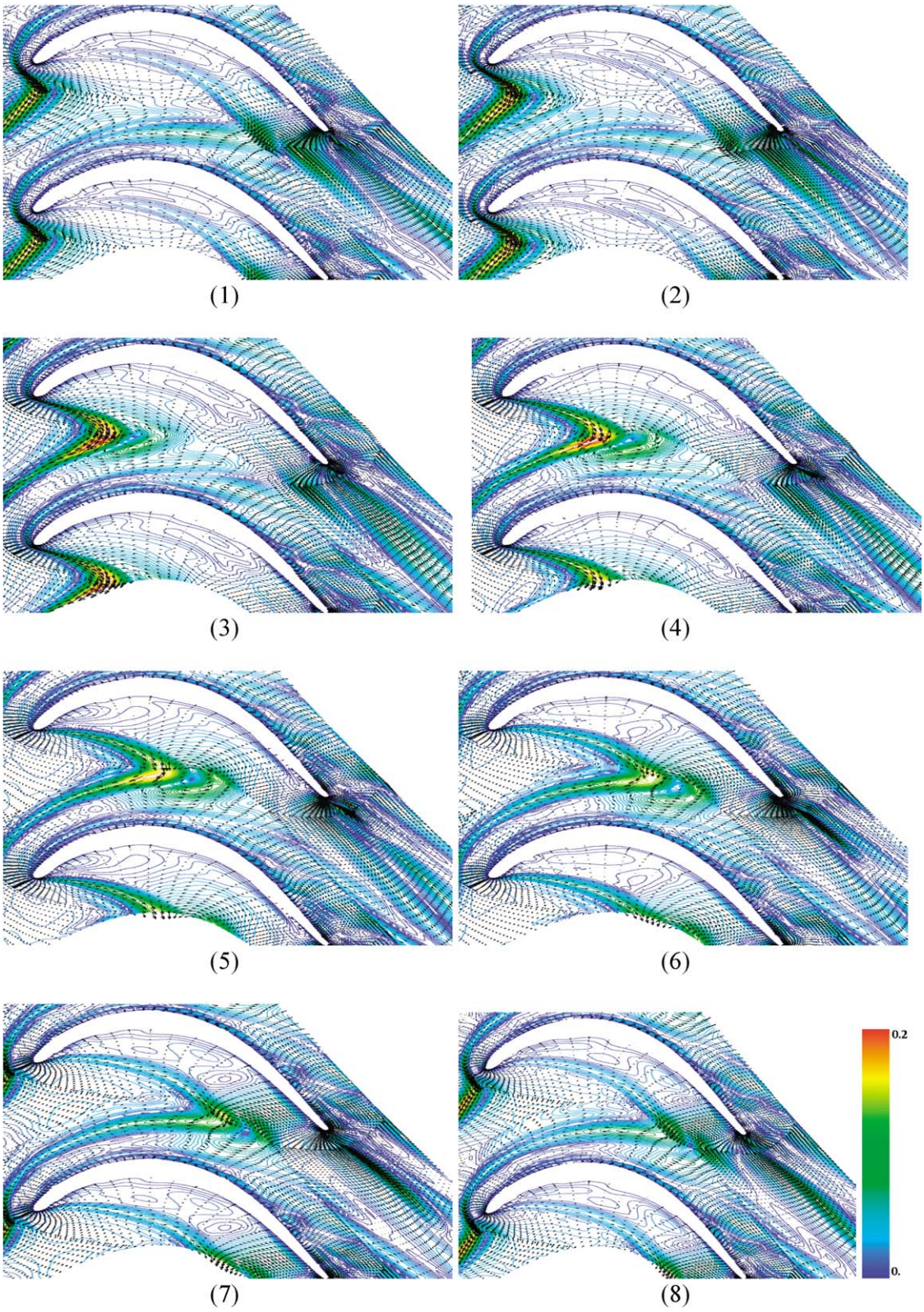

Fig. 8. Velocity fluctuations at midspan during a full time period.

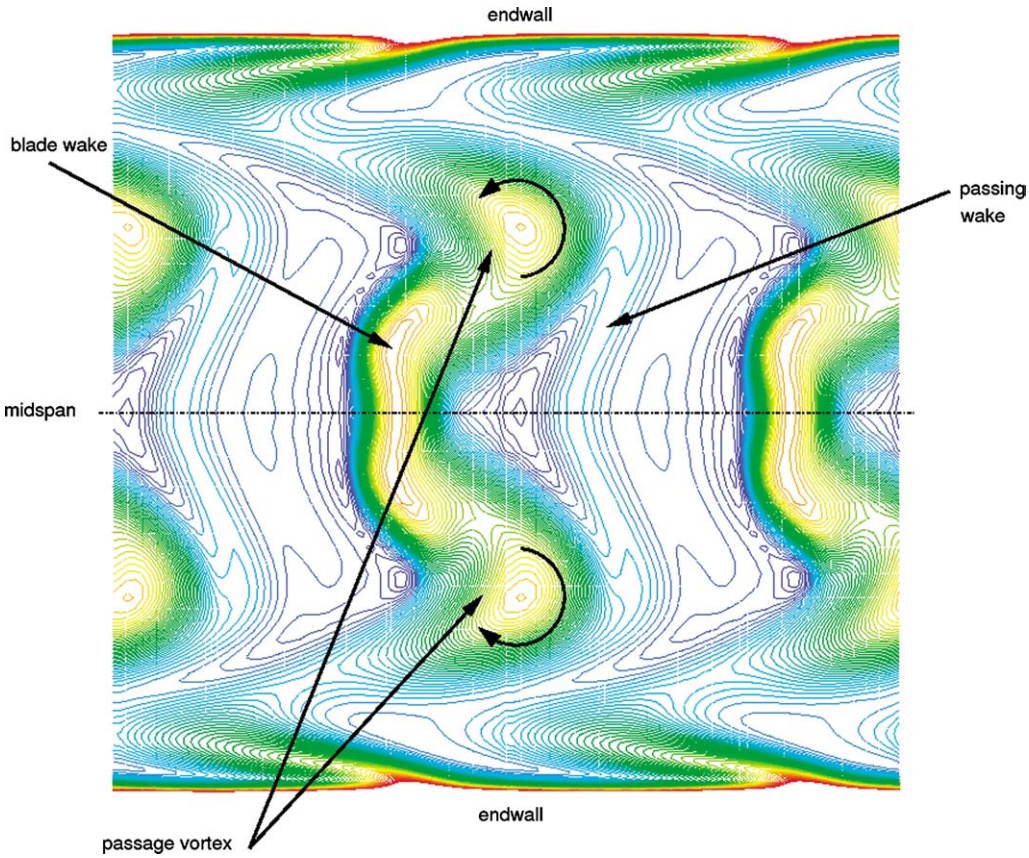

Fig. 9. Losses behind the trailing edge.

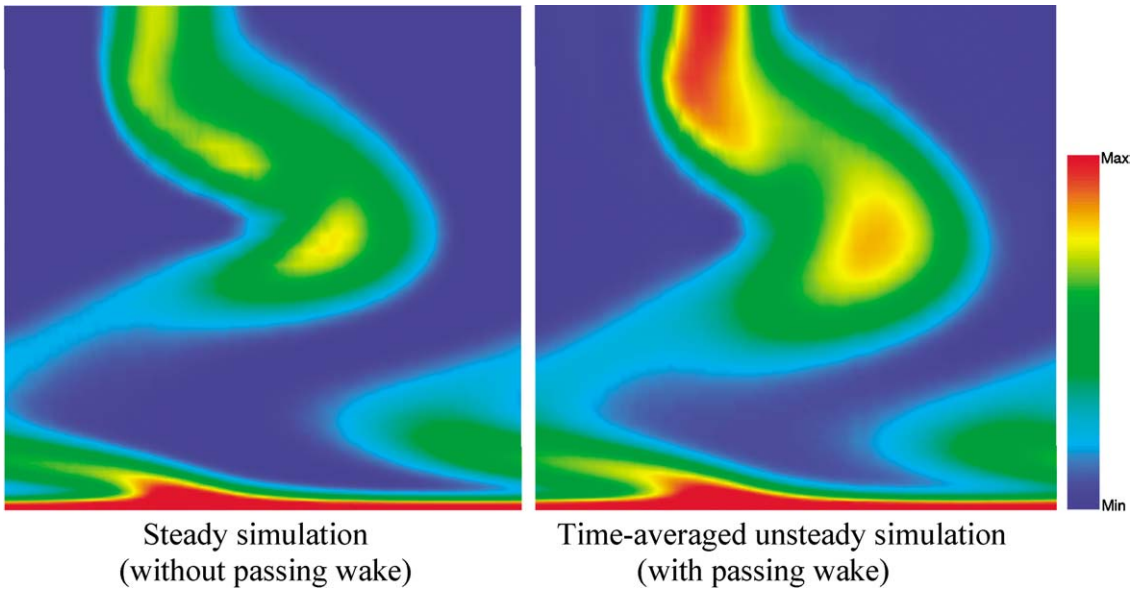

Fig. 10. Losses behind the trailing edge.

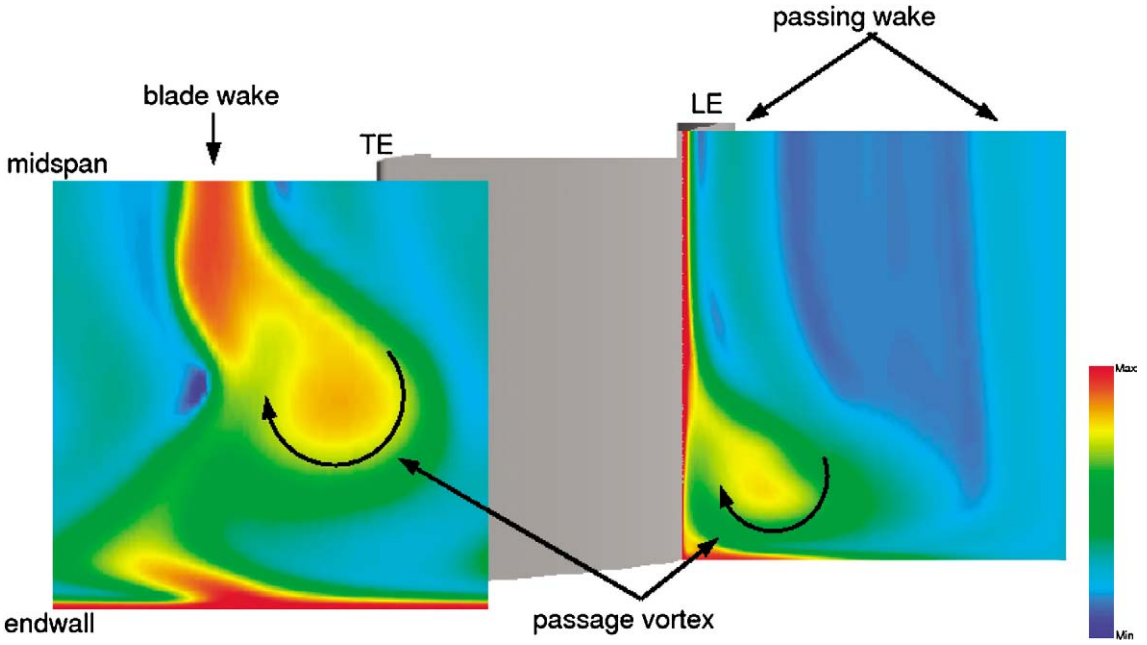

Fig. 11. Entropy evolution.

the pressure side to the suction side. The passing wake-blade interaction creates two counter-rotating vortices which contribute to the flow convection too. The blade boundary layer and downstream wake are strongly influenced. The beating of the blade wake has been observed.

The physical analysis allows to separate the main origins of the losses. This study shows that, when the passage vortex is the main origin of the losses near the endwall, its development is not influenced by the passing wake.

Moreover, this work contributes to show that an unsteady boundary condition is able to reproduce the physical phenomena and then avoid a complete stage unsteady calculation.

Acknowledgements

The simulations were performed on the NEC-SX5 of the computer center IDRIS.

References

[1] S.E. Gorrell, T.H. Okiishi, W.W. Copenhaver, Stator–rotor interactions in a transonic compressor: Part 1 – Effect of blade-row spacing on performance, ASME Turbo Expo 30494, 2002.
[2] S.E. Gorrell, T.H. Okiishi, W.W. Copenhaver, Stator–rotor interactions in a transonic compressor: Part 2 – Description of a loss producing mechanism, ASME Turbo Expo 30494, 2002.
[3] T.V. Valkov, C.S. Tan, Effects of upstream rotor vortical disturbances on the time-average performance of axial compressor stator, Part 1: Framework of technical approach and wake-stator blade interactions, ASME 98-GT-312, 1998.
[4] H.P. Hodson, in: Blade Row Interference Effects in Axial Turbomachinery Stages, in: VKI Lecture Series, vol. 1998-2, Von Karman Institute for Fluid Dynamics, 1998.
[5] F. Eulitz, K. Engel, Numerical investigation of wake interaction in a low pressure turbine, ASME 98-GT-563, 1998.
[6] C. Dano, Evaluation de modèles de turbulence pour la simulation d'écoulements tridimensionnels instationnaires en turbomachines, PhD thesis 2003-n°05, Ecole Centrale de Lyon, 2003.
[7] B.R. Smith, The *k–kl* turbulence model and wall layer model for compressible flows, AIAA paper 90-1483, 1990.
[8] E. Boletis, C.H. Sieverding, Experimental study of the three-dimensional flow field in a turbine stator preceded by a full stage, ASME J. Turbomachinery 113 (1991).
[9] O.P. Sharma, G.F. Picket, R.H. Ni, Assessment of unsteady flows in turbines, ASME J. Turbomachinery 114 (1992).
[10] A.H. Epstein, M.B. Giles, T. Shang, A.K. Sehra, Blade row interaction effects on compressor measurements, Unsteady Aerodynamic Phenomena in Turbomachines, AGARD-CP-468, 1989.
[11] T. Coton, T. Arts, M. Lefebvre, N. Liamis, Unsteady and calming effects investigation on a very high lift LP turbine blade: experimental analysis, ASME Turbo Expo 30227, 2002.

[12] T. Arts, M. Lambert de Rouvroit, Aerothermal performance of a 2D highly loaded transonic turbine nozzle guide vane: a test case for inviscid and viscous flow computations, ASME J. Turbomachinery 114 (1992).
[13] B.R. Smith, A near wall model for the *k–l* two-equation turbulence model, AIAA paper 94-2386, 1994.
[14] C.G. Speziale, On nonlinear *k–l* and *k–e* models of turbulence, J. Fluid Mech. 178 (1987).
[15] A.M. Vuillot, V. Couailler, N. Liamis, 3D turbomachinery Euler and Navier–Stokes calculation with multi-domain cell-centered approach, AIAA paper 93-2576, 1993.
[16] N. Marciniak, P. Kulisa, B. Lakshminarayana, Development and assessment of thermal flux model for computation of turbine heat transfer, 13th ISABE 97-7161, 1997.
[17] L. Castillon, E. Laroche, O. Sgarzi, Unsteady three-dimensional Navier–Stokes analysis of a hot streak transport through an axial high pressure turbine stage, ISABE 2003-144, 2003.
[18] B. Lakshminarayana, Davino, Mean velocity and decay characteristics of guide-vane and stator blade wake of an axial flow compressor, ASME J. Engrg. Power 102 (1980).
[19] R.X. Meyer, The effects of wakes on the transient pressure and velocity distributions in turbomachines, ASME J. Basic Engrg. 80 (1958).
[20] H.P. Hodson, W.N. Dawes, On the interpretation of measured profile losses in unsteady wake-turbine blade interaction studies, J. Turbomachinery 120 (1998).
[21] H.P. Hodson, Measurements of wake-generated unsteadiness in the rotor passages of axial flow turbines, ASME J. Engrg. Gas Turbines and Power 107 (1985).
[22] P. Cardamone, P. Stadtmüller, L. Fottner, Numerical investigation of wake-boundary interaction on highly loaded LP turbine cascade blade, ASME Turbo Expo 30367, 2002.
[23] C. Casciaro, M. Treber, M. Sell, Unsteady transport mechanisms in an axial turbine, J. Turbomachinery 122 (2000).